Biosensors and Bioelectronics 141 (2019) 111441

Contents lists available at ScienceDirect

Biosensors and Bioelectronics

journal homepage: www.elsevier.com/locate/bios

Electrospun tin (IV) oxide nanofiber based electrochemical sensor for ultra-sensitive and selective detection of atrazine in water at trace levels

Patta Supraja[a], Suryasnata Tripathy[a], Siva Rama Krishna Vanjari[a], Vikrant Singh[b], Shiv Govind Singh[a,*]

[a] Department of Electrical Engineering, Indian Institute of Technology Hyderabad, 502285, India
[b] School of Medicine, University of California Davis, USA

ARTICLE INFO

Keywords:
Atrazine
SnO_2 nanofibers
Electrospinning
Covalent chemistry
Pesticide

ABSTRACT

Atrazine, a class 3a carcinogen, is a pesticide of chloro triazine family and is known to severely affect the human endocrine system upon consumption. The toxic effects of atrazine cause damage not only to the humans but also to animals and plants. In lieu of the detrimental effects of atrazine on environment, it is essential to develop a sensor platform capable of its detection in water. Here, we propose ultrasensitive electrochemical detection of atrazine using electrospun SnO_2 nanofibers. In this study, the nanofibers have been characterized using Field Emission Spectroscopy, X-ray diffraction analysis (XRD), X-ray photoelectron spectroscopy (XPS), UV-Vis-NIR spectroscopy and Fourier transform infrared spectroscopy (FTIR). Using a label-free transduction, we have detected atrazine in fairly low concentrations, with the limit of detection being 0.9 zM and the sensitivity being 4.11 (μA/μM)/cm^2, in a wide dynamic detection range varying from 1 zM to 1 μM. Furthermore, we have reported atrazine detection in trace levels in spiked real time water samples, which is an essential step in ensuring that the sensing platform can be deployed for practical applications. In addition to this, the sensor exhibits excellent selectivity, reasonable stability (when stored at 4 °C), and good interference-resistance.

1. Introduction

Pesticide is the mixture of organic substance used to prevent, destroy or migrate any pest. In agriculture sector crops, seeds are protected by pesticides. Cytotoxic and carcinogenic behavior of pesticides results in infertility, neurological disorders, and respiratory problems in humans. Usage of pesticide may be in small area but it can affect large areas by moving through air or seeping in soil or through water bodies after dissolving in water. The most widely used pesticides are from the chloro-triazine family. Atrazine (1-chloro-3-ethylamino-5-isopropylamino-s- triazine) is the most broadly used pesticide of triazine family due to its high efficiency (Javaroni et al., 1999). In 1958, it was first introduced as a herbicide for dicotyledons (Hartley and Kidd, 1987). Due to biodegradation by microbes, the half-life time of atrazine in soil is 261 days, however the degradation takes much longer time in water due to low solubility (Shiu et al., 1990). Consumption of atrazine rich water causes several health problems like endocrine disruption, hormone disruption, in addition to the risk of breast and prostate cancer (Aktar et al., 2009; Neumann et al., 2004; Vogel et al., 2015). Children are the most adversely affected, whereas exposure to atrazine during pregnancy results in low fetus weight, limb/urinary/heart defects. Further, long exposure to high level concentrations results in reduced survival of fetus. According to the US Environmental Protection Agency, maximum acceptable level of atrazine concentration in drinking water is 3 parts per billion (Maleki et al., 2007; Kolpin et al., 2000), though long-term exposure to even lower concentrations also affects human endocrine system severely. The detrimental effects of atrazine is not limited to humans, rather it also adversely impacts plants and animals. On account of the above mentioned pernicious effects on the environment, it is essential to facilitate the detection of atrazine in water. In general, towards the detection of atrazine, several analytical techniques have been employed in the past, such as Gas chromatography (Tang et al., 2005; Williams et al., 2014; Yokley and Cheung, 2000), high performance liquid chromatography (Panuwet et al., 2008; Trachta et al., 2004) and capillary zone electrophoresis (Penmetsa et al., 1996). However, the usage of these methods is limited due to cost, time, sample preparation protocols and non-amenability to miniaturization. As a result, these methods are not suitable for real time, on site in-situ detection of atrazine in water. Hence, different avenues need to be explored. In this context, immunosensors stand out as powerful

* Corresponding author. IIT Hyderabad, Kandi, 502285, India
E-mail addresses: ee17resch01006@iith.ac.in (P. Supraja), ee14resch11017@iith.ac.in (S. Tripathy), svanjari@iith.ac.in (S.R. Krishna Vanjari), vssingh@ucdavis.edu (V. Singh), sgsingh@iith.ac.in (S.G. Singh).

https://doi.org/10.1016/j.bios.2019.111441
Received 27 March 2019; Received in revised form 5 June 2019; Accepted 14 June 2019
Available online 16 June 2019
0956-5663/

alternatives for on-site detection of molecules. In brief, immunosensors are based on antibody-antigen interactions, wherein antibodies specific to target antigens are used as capturing agents. These capturing molecules are often attached on to sensing surfaces/materials, such that the desired antibody-antigen binding event can be transduced into a measurable physical entity. Here, the limit of detection of the immunosensor and the strength of the transduced signal depend on the antibody-antigen binding efficiency. Among several transduction principles used in immunosensing (such as optical (Reardon, 2012), electrochemical (Mazzei and Botre, 2007) and piezoelectric transduction (Jia et al., 2013) methods), the electrochemical approaches are preferred due to their high sensitivity and small response time.

Keeping this in mind, in this work we are reporting an ultrasensitive label free electrochemical transduction based immunosensors for detection of trace amounts of atrazine. In a previous communication, we have reported the electrochemical detection of atrazine, wherein low bandgap manganese oxide (Mn_2O_3) nanofibers were used as the transducing material (Supraja et al., 2019). In contrast, herein, we have used high bandgap tin oxide nanofibers (SnO_2) as the sensing material, which as opposed to the semiconducting action of Mn_2O_3, provide a switching action. Traditionally, switching action of high bandgap nanomaterials (such as ZnO, NiO, SnO_2, MnO_2, CeO_2, Cu_2O etc.,) has been widely employed in electrochemical immunosensing. In light of this, in this report, we have opted to use a high bandgap nanomaterial (SnO_2) for the desired immunosensing. In Table 1, we have compared the performance of the reported work with previously reported literature. As can be inferred, in terms of the limiting detection, the proposed work provides a clear advantage. Note, the nanofibers used in this work are synthesized using electrospinning (Tripathy et al., 2017; Brince Paul et al., 2016), with subsequent high temperature calcination. The detailed protocol of the nanofiber synthesis is provided in subsequent sections. The schematic representation of the proposed nano biosensing platform for detection of atrazine is shown in Fig. 1.

2. Methods and materials

2.1. Materials and apparatus

In this work, Tin (IV) acetate ($Sn(CH_3COO)_4$), Polyacrylonitrile (PAN), N, N-dimethylformamide (DMF), 10 mM Phosphate Buffer Saline (pH-7.4), N- hydroxysuccinimide (NHS), Mercaptopropionic acid (MPA), 3-(Ethylimino methyleneamino)- N,N-dimethylpropan-1-amine (EDC) and Bovine Serum Albumin (BSA) were purchased from Sigma Aldrich. All the above mentioned chemical reagents were of analytical grade and used as they received without any additional purification. Atrazine and anti-atrazine (AB30533) antibody were purchased from Sigma Aldrich and Abcam (United Kingdom) respectively. Aliquots of atrazine were prepared in PBS solution. Throughout this study we used Deionized water (resistivity 18.2 MΩ-cm). Glassy carbon electrodes, glasswares were purchased from Sinsil International Mumbai and Hychem Laboratories respectively.

Optical properties of electrospun and calcinated nanofibers were analyzed by using UV-Vis-NIR spectroscopy (PerkinElmer; Lambda-750). Ability to functionalize the carboxylic group on to the SnO_2 nanofibers after MPA treatment has tested with Fourier transform infrared spectroscopy (FTIR) (PerkinElmer; Model- Spectra 100). Elemental as well as oxidation state analysis of SnO_2 nanofibers was performed using X-ray photoelectron spectroscopy (XPS; ULVAC-PHI; Model pHI 5000 VersaProbell). The morphological study of SnO_2 nanofiber mat before and after calcination were accomplished with scanning electron microscope (SEM; pro X, Phenom World), and field emission scanning electron microscope (FE-SEM; Supra 400VP, Zeiss, Germany). The crystallographic analysis of calcinated SnO_2 nanofibers was analyzed with X-ray diffraction instrument (XRD; Bruker Axs, X-ray system with Cu Kα radiation, λ = 1.54 Å). All electrochemical measurements in this study were carried out by using well known electrochemical analyzer

Table 1
Comparison of proposed sensing platform with reported literature.

Type of Detection	Immobilization Technique	Method of Detection	Detection limit	Reference
Label free	Bio functionalization of atrazine with 2d-BSA selectively on surface of the gold electrodes by thiol chemistry. *N*-acetylcysteamine to cover the gold electrodes	EIS	40 ng L^{-1}	Ramón-Azcón et al.,2008
Label free	Immobilization of antibody on to the gold electrode, which is modified with NTA substituted polypyrrole film. (polypyrrole NTA + Cu2 ions + Antibody)	CV and EIS	10 pg mL^{-1}	Ionescu et al.,2010
Label free	Coating of magnetic particles (magnetic monolayer) with streptavidin on to the gold electrodes.	Faradaic Impedance Spectroscopy and CV	10 ng mL^{-1}	Helali et al.,2006
Surface Plasmon Resonance (SPR)	Covalent immobilization of analyte on gold coated electrode by alkanethiol self-assembled monolayer	SPR	20 ng L^{-1}	Farré et al.,2007
Labelled	Immobilization of monoclonal antibody on to the carbon electrode which is modified with Biodyne C membrane. Glucose oxidase which is labelled with HRP used for Catalases and substrate scavenging.	Amperometric SPE	2 ng L^{-1}	Keay and McNeil.,1998
Labelled	Immobilization of HRP labelled single chain antibodies on to the screen printed electrode which is made up of polyaniline, polyvinyl sulfuric acid and carbon composite.	Amperometric SPE	0.1 μg L^{-1}	Grennan et al.,2003
Label free	Integration of molecularly imprinted nanofilms (MAPA + VIM + EGDMA) with SPR	AFM, ellipsometry and CA (Change in absorbance)	0.091 nM	Saylan et al.,2017
Optical fiber	Coating of 40 nm thick Ag layer on unclad optical fiber followed by coating of molecular imprinted polymer with atrazine as template molecule	Spectral interrogation method Shift in the resonance wavelength	19.2 pM	Agrawal et al.,2016
Label free	Covalent immobilization of atrazine antibody through the functionalization of SnO2 nanofibers by using MPA, (EDC-NHS), BSA.	DPV and CV	0.9 zM	This work

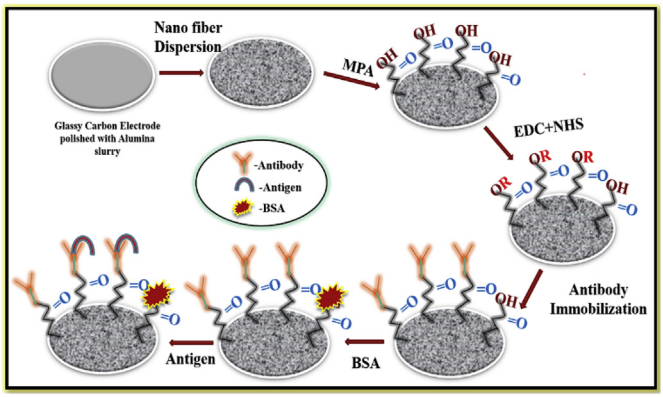

Fig. 1. Schematic illustration of the proposed biosensing platform.

CHI660E (CH Instruments, TX, USA). In this electrochemical study standard Ag/AgCl, platinum and glassy carbon (GCE- 3 mm diameter) electrodes were used as reference, counter and working electrodes respectively. 5 mM potassium ferro/ferricyanide redox couple [[Fe $(CN)_6]^{4-/3-}$] was used as electrolyte in all our electrochemical studies.

2.2. Methods and protocols

2.2.1. Synthesis of SnO_2 nanofibers

In this work, SnO_2 nanofibers were synthesized by the well-known electrospinning method. Briefly, a PAN-DMF polymer solution (w/w) was prepared by adding 7% of PAN powder to DMF and stirred for 90 min at 60 °C. To this homogeneous mixture, 5% of Tin (IV) Acetate was added slowly and allowed it to mix properly by using magnetic stirring technique. The homogeneous precursor and polymer blend solution was transferred into syringe (5 mL capacity) which has 26 gauge needle. An electric field of 1.6 KV/cm was applied between the tip of 26 gauge needle and collector plate (grounded) which was kept 15 cm distance from the tip of needle. The electrospinning was performed at a feeding rate of solution was 1.5 mL per hour for 4 hours, following which a thick non-woven fiber mat was collected. The nanofiber mat was subsequently calcinated at 550 °C in air for 3 hours by using a muffle furnace.

2.2.2. Electrode preparation protocol

The electrodes for detecting atrazine were prepared by immobilizing anti-atrazine antibody on to SnO_2 nanofiber modified GCE. As a first step towards this, the working electrode (GCE) was cleaned with aluminum slurry (0.05 μm and 0.3 μm), followed by washing with DI water. The electrodes were dried in air at 60 °C. Later, these electrodes were surface modified with 6 μL of nanofiber dispersion (5 mg mL^{-1}), which was prepared by the addition of 5 mg SnO_2 powdered nanofiber to DMF and ultrasonicating the mixture for 40 min. The nanofiber coated GCEs were allowed to dry for 2 hours in air at 60 °C. Afterwards, surface functionalization of the GCE/SnO_2 electrodes was carried out by incubating them in MPA (10 mM - diluted in ethanol) for 18 hours. MPA treatment results in the formation of a self-assembled monolayer on the SnO_2 nanofibers, which provides us with an abundance of carboxyl (–COOH) groups. This is a critical step in the bioelectrode design as presence of the –COOH functional group is essential for immobilization of anti-atrazine antibody. Subsequently, activation of these carboxyl functional groups is ensured by EDC-NHS treatment. In brief, 6 μL of EDC-NHS mixture (1:1, by volume) was drop-casted on to the working electrode (GCE/SnO_2/MPA) and they were left as such for 4 hours at room temperature. These surface functionalized and activated GCEs (GCE/SnO_2/MPA/EDC-NHS) were then treated with 4 μL of atrazine antibody (1 μg mL^{-1}) for 12 hours at 4 °C. This resulted in the formation of peptide bonds (CO–NH) between the Carboxyl group and amine group of antibody, leading to the immobilization of anti-atrazine on to the GCE. Following the incubation, the GCE/SnO_2/MPA/EDC-NHS/Antibody electrodes were thoroughly washed with PBS and air dried at 37 °C. The electrodes were then subjected to a BSA treatment, such that the activated sites on the electrode that are not occupied by the antibodies, would be made unavailable for the target analytes. The bioelectrode was stored at 4 °C whenever it was not in used. Fig. 1 shows the schematic illustration of proposed atrazine biosensing platform.

2.2.3. Electrochemical methods

The label-free detection of atrazine was carried out by using electrochemical methods i.e. Differential Pulse Voltammetry (DPV) and Cyclic Voltammetry (CV). The cyclic voltammetry analyses were performed in the voltage range of −0.4 V to +0.8 V, with a voltage scan rate of 80 mV/S and sample interval of 1 mV. DPV was also carried out in the same range as CV with a pulse width of 5 ms and sampling duration of 16.7 ms. All the above mentioned electrochemical measurements were accomplished with three electrode system described previously, in 10 mL of PBS electrolyte containing 5 mM of $[Fe(CN)_6]^{4-/3-}$ redox couple. The atrazine detection measurements (DPV) were carried out using a sequential addition method, wherein 100 μL of analyte-spiked PBS buffer was added sequentially to the electrochemical cell. Post the analyte addition to the bulk electrolyte, and prior to recording the DPV, the system was allowed to stabilize for sufficient amount of time (900 seconds), during which the analyte molecules diffuse towards the surface of working electrode and the antibody-antigen reaction takes place. The initial stock solution was prepared by adding known weight of atrazine to the 10 mL of solvent, which was later diluted to lower concentrations following a serial dilution protocol.

2.2.4. Protocol for stability, selectivity and interference studies

Stability analysis of the proposed atrazine biosensor was performed by storing the antibody modified electrode (GCE/SnO_2/MPA/EDC-NHS/Antibody) at 4 °C for 28 days, where the electrode response was periodically monitored (once in every 7 days). For evaluating the selectivity of the bioelectrodes, the electrode's response to 1 μM of Urea, Glucose, Antibiotic (ANTB), Bovine serum albumin (BSA), Human serum albumin (HSA), Sodium ions (Na^+) and Melamine (MLMN) was recorded separately. Towards this, all the stock solutions of target chemicals were prepared by adding known weight of the chemical in 10 mL of PBS, followed by serial dilution to prepare aliquots with lower concentrations. We also performed interference studies to evaluate the efficiency of the proposed sensing platform. Specifically, we first recorded the sensor's response to identical concentrations of the interfering compound (urea and glucose) and the atrazine antibody. Subsequently, the biosensor's response to a 1:1 mixture of atrazine and the interfering compound was recorded. A more detailed discussion regarding this is provided in section 3.5 of the manuscript.

3. Results and discussion

3.1. Assessment of nanofiber characteristics

Morphological analysis of electrospun SnO_2 nanofibers before and after calcination is shown in Fig. 2(a) and (b) respectively. Pre-calcination, SnO_2 nanofiber morphology is smooth as well as uniform with diameter in the range 500 nm. Calcination of the composite fiber mat at 550 °C results in the formation of crystalline SnO_2 fibers with diameter in the range of 200 nm. This shrinkage in the fiber dimension from pre calcination to post calcination is attributed to the evaporation of PAN at 400 °C. Fig. 2(c) shows the XRD analysis of calcinated nanofibers. Characteristic peaks for SnO_2 are observed at angles 26.1, 31.9, 37.1, 41.4, 49.5, 54.0, 57.5, 60.6, 63.4 which corresponding to (110), (101), (200), (111), (210), (220), (002), (310), (112) crystal planes respectively. The observed peaks are well correlated with previously reported

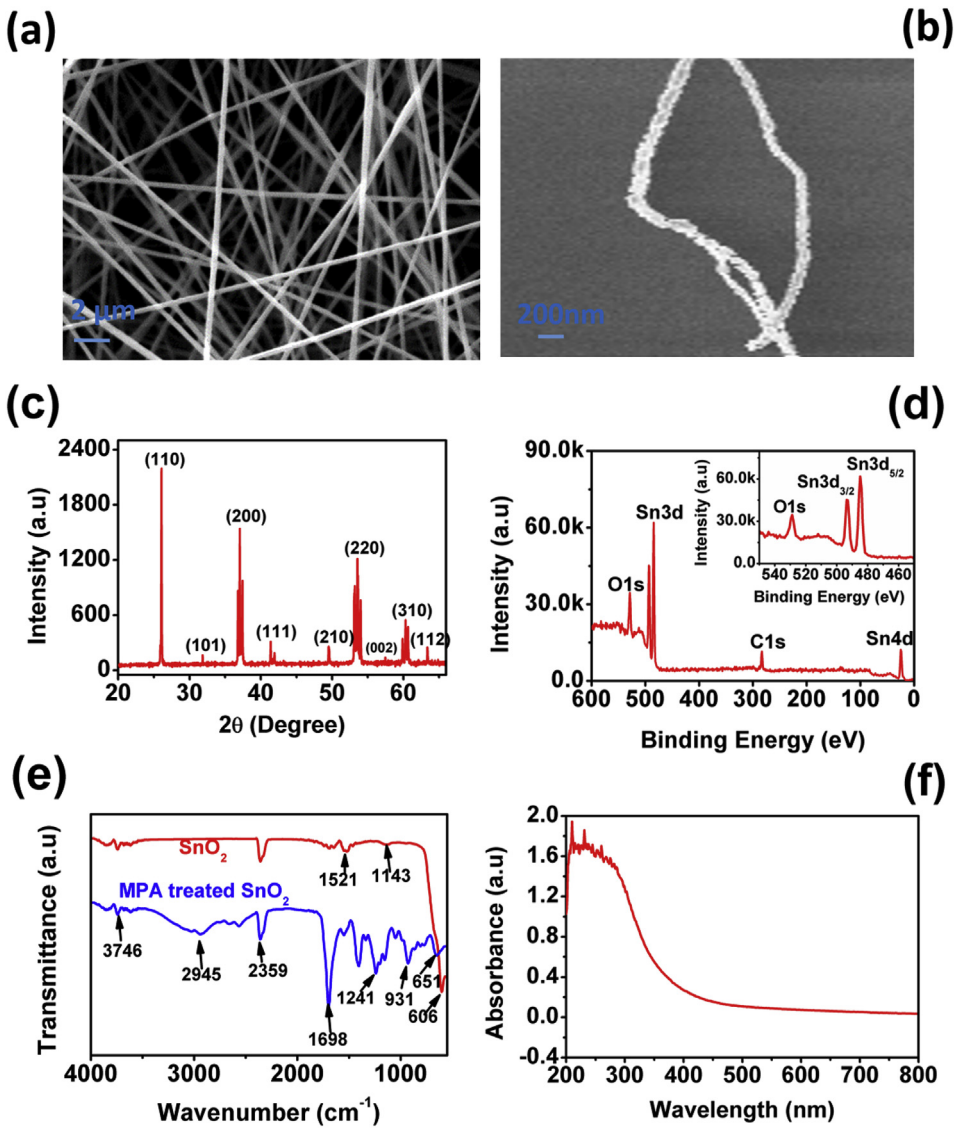

Fig. 2. FESEM images of SnO_2 nanofiber mat (a) before calcination (b) after calcination in air at 550 °C, (c) XRD analysis (d) XPS analysis (e) FTIR analysis (f) UV–VISIBLE spectroscopic analysis of electrospun SnO_2 nanofibers.

literature (Cheng et al., 2014). XPS elemental analysis of the calcinated nanofibers, as demonstrated in Fig. 2 (d), helps us to identify the exact oxidation state of tin. Peaks at 484.49 and 493.24 eV corresponds to Sn $3d_{5/2}$, $3d_{3/2}$ which confirming the oxidation state of Sn as +4. The position (binding energy) of peaks of Sn 3d, Sn 4d, O 1s confirming the formation of SnO_2. Furthermore, the characteristic peak of O 1s orbital was observed at 529.96 eV, confirming the oxidation process. Fig. 2(d) depicts the characteristic peaks of synthesized SnO_2 XPS data. Characteristic peaks of Sn (IV) phase is very well correlated with reported literature (Dou et al., 2011), indicating successful synthesis of SnO_2 nanofibers. Fig. 2(e) shows FTIR transmittance spectrum of SnO_2 nanofibers and the MPA treated SnO_2 nanofibers. To immobilize the desired antibody on to the nanofiber surface, it is necessary to ensure the introduction of carboxylic functional groups via Mercaptopropionic acid (MPA) treatment. To confirm this surface functionalization, we have opted for FTIR analysis for both MPA treated and bare nanofibers. The characteristic peaks of SnO_2 has observed in the range 500–700 cm^{-1} range. The broad peak in the range 2800–3500 cm^{-1} corresponding to the MPA treated nanofibers is due to the O–H stretching and peak at 1701.73 cm^{-1} is characteristic to the C═O stretching vibrations. The C–O bond stretching vibrations can be confirmed by the peaks in the range 1000–1400 cm^{-1}. All the peaks corresponds to carboxylic functionalization bonds has very well correlated with literature (Nehru and Sanjeeviraja, 2014). The FTIR analysis of the MPA treated nanofibers is a strong indicator of the formation of desired functional groups. Fig. 2(f) shows UV–Vis absorption spectrum of SnO_2 nanofibers. Absorbance is almost zero in the visible range (400–800 nm) and maximum absorbance has observed at wavelength 231 nm (Dharmaraj et al., 2006).

3.2. Electrochemical studies of bioelectrode

Electrochemical analysis of anti-atrazine modified working electrode has been performed using CV and DPV. After each step of the bioelectrode synthesis protocol, the working electrode's response was analyzed. Fig. 3(a) shows the differential pulse voltammogramm for the cleaned working electrode (bare GCE), SnO_2 nanofiber modified GCE (GCE/SnO_2), surface functionalized GCE (GCE/SnO_2/EDC-NHS), antibody immobilized GCE (GCE/SnO_2/EDC-NHS/Antibody) and BSA blocked working electrode (GCE/SnO_2/EDC-NHS/Antibody/BSA). As can be seen, the oxidative peak current for bare GCE is 168.6 μA and potential corresponding to peak is 185.1 mv. After surface modification of the electrode with SnO_2 nanofibers, the peak current decreased to 31.99 μA and peak shifted to higher potential, which indicates a

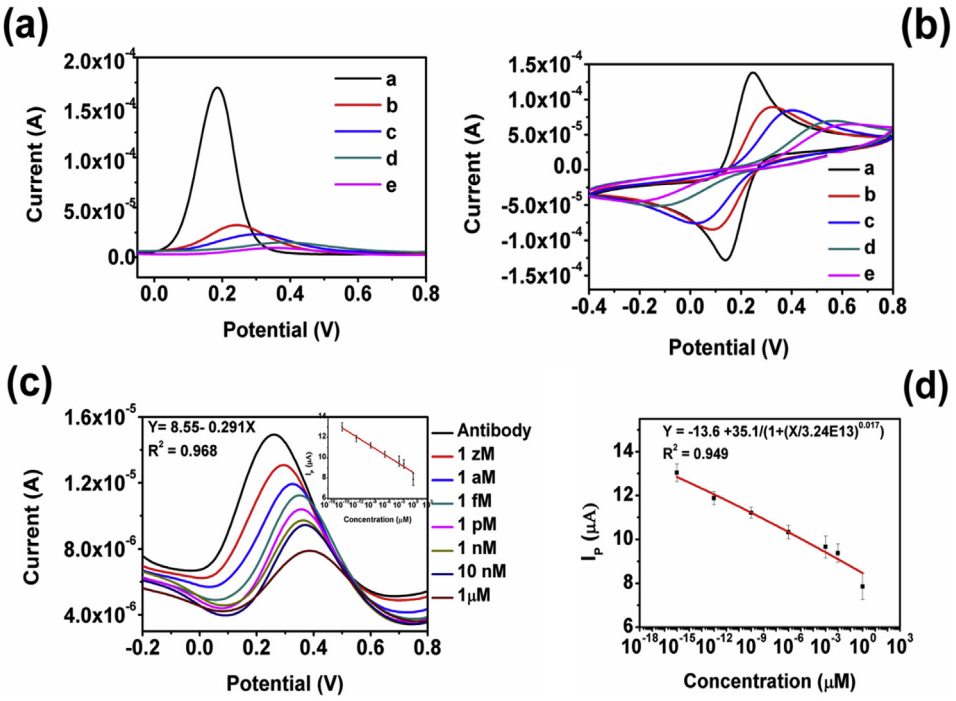

Fig. 3. (a) DPV (b) CV electrochemical analysis of bioelectrode at each stage of bioelectrode preparation (Inset **a**. GCE, **b**. GCE/SnO_2, **c**. GCE/SnO_2/EDC-NHS, **d**. GCE/SnO_2/EDC-NHS/Antibody, **e**. GCE/SnO_2/EDC-NHS/Antibody/BSA (c) DPV electrochemical response of bioelectrode (GCE/SnO_2/EDC-NHS/Antibody/BSA) with respect to atrazine concentration and inset shows dynamic linear curve fitting as function of atrazine concentration (d) Calibration curve of peak currents with logistic sigmoidal curve fitting.

decrease in the electron transfer kinetics. This behavior can be accredited to the semiconducting behavior of SnO_2 nanofibers. Post-immobilization of the antibody by covalent chemistry after MPA and EDC-NHS treatment, the electrode characteristics also follow a similar trend due to insulating nature of the attached biomolecule. We also performed cyclic voltammogramm analyses to verify the results obtained via differential pulse voltammetry. As shown in Fig. 3(b), the CV obtained for GCE, GCE/SnO_2, GCE/SnO_2/EDC-NHS, GCE/SnO_2/EDC-NHS/Antibody and GCE/SnO_2/EDC-NHS/Antibody/BSA demonstrate a similar trend of change in charge transfer resistance. The charge transfer resistance as seen at the electrode surface is an indicator of the overall reaction kinetics, and an increase in the same symbolizes a reduction in the electron transfer rate at the electrode-electrolyte interface. As evident from the CV plots, each step of surface modification reduces the overall rate kinetics at the working electrode's surface, a trend which was already established by the differential pulse voltammogramm presented in Fig. 3(a).

3.3. Detection of atrazine in spiked PBS buffer

Electrochemical analysis of the anti-atrazine antibody immobilized bioelectrode was performed using DPV, against various concentrations of atrazine. Fig. 3(c) demonstrate the differential pulse voltammogramm with inset linear fitting of data over a wide range of atrazine concentration, 1 zM - 1 μM. In relation to this, we have performed a blank response analysis, so as to ensure that the change in the bioelectrode response is indeed a resultant of the antibody-antigen interaction, and is independent of the working buffer (see supplementary material).

The differential pulse voltammogramm presented in Fig. 3(c) indicates a constant decrease in the reaction kinetics at the working electrode surface with increasing target concentration. This can be explained by correlating the electron transfer to the adsorption layer thickness. With increasing concentration, the amount of adsorbed atrazine increase, thereby increasing the overall adsorption layer, which in turn hinders the electron transfer process. The electrons now require additional energy to overcome this additional electrical barrier, and thus the resulting peak current goes down. This phenomenon can be attributed to the non-conducting nature of the atrazine molecule, which when adsorbed, enhances the overall electrical barrier seen by the electrons Fig. 3(d) shows the variation of the anodic peak currents with atrazine concentration, along with a four parameter sigmoidal curve fitting. The fitting function used here is given as:

$$Ip = a2 + \frac{(a1 - a2)}{1 + \left(\frac{x}{x0}\right)^{p}}$$

where a1,a2,x, x0 and p correspond to the minimum asymptote, maximum asymptote, concentration of atrazine, atrazine concentration corresponding to 50% of the maximum signal change (which is known as inflection point) and slope at the inflection point of the sigmoid, respectively. We have calculated the limit of detection and the sensitivity of the proposed sensor, using the 3.3σ/slope and slope/(area of electrode) respectively, where σ is the standard deviation of blank measurement. The proposed biosensor accounts for good sensitivity of 4.11 (μA/μM)/cm^2 with a wide dynamic detection range varying from 1 zM to 1 μM. The limit of detection (LOD) of the proposed sensor is found to be 0.9 zM. For such low ranges of detection, in case of electrochemical biosensors, as the bulk concentration of the analyte is equal to the surface concentration, diffusion does not play any major role in deciding the overall response, and hence can be neglected. In these cases, the sensor's response can be explained in terms of the heterogeneity of the working-electrode. For heterogeneous electrodes, adsorption of any analyte on to the electrode's surface results in a more prominent change in the rate kinetics as compared to the homogeneous electrodes. This affects the activation barriers at the electrode-electrolyte interface, thereby affecting the charge transfer coefficient, α. Change in α is reflected exponentially in the exchange current density, which in an indicative of the kinetics as described by the Butler Volmer's equation. As a result, even a small change in the surface condition results in an appreciable change in the current density, thereby making the detection of fairly low analyte concentrations possible (Fu et al., 2016; Rahi et al., 2015; Amiri et al., 2017). In our case, the use of nanofibers introduces heterogeneity on the working electrode surface, which facilitates the ultra-low detection. Also, for these semiconducting nanomaterials, any adsorption on the surface occurs within the Debye length, which drastically alters their electronic properties (Smith et al., 2016; Stern et al., 2007). As a result, even for a small alteration in the

surface condition, which may have been caused by the adsorption of a few analyte molecules, the corresponding change in the kinetics would be significant. We believe, in the present case, a combination of high surface heterogeneity and semiconducting properties of the nanofibers is responsible for positive detection even though the number of analyte molecules is fairly small.

3.4. Detection of atrazine in spiked water samples

Atrazine is used by farmers as pesticide for the cultivation of crops. In the process, atrazine dissolves in water and moves through the water bodies. So, it is essential to test the ability of the proposed sensor to detect atrazine in real water samples. Towards this, we investigated the sensor's efficiency against atrazine spiked mineral water and ground water.

3.4.1. Detection of atrazine in mineral water

Initially known weight of atrazine was added to 1 mL of mineral water and the resulting mixture was ultra-sonicated for 60 min to obtain a homogeneous 10 μM concentrated Aliquot. Lower concentrations of the target sample were prepared through serial dilution protocol. The electrochemical response of the bioelectrode upon introduction of the target atrazine solution to the bulk electrolyte was recorded with DPV. Upon introduction to the electrolyte, atrazine molecules diffuse towards the surface of the bioelectrode and get attached to the anti-atrazine antibody on account of their affinity. As concentration of atrazine increased, the resulting peak current decreased and the potential corresponding to the peak current shifted towards higher voltages. Fig. 4(a) shows the differential pulse voltammograms indicating detection of atrazine in mineral water, along with a linear fitting approximation (inset). The linear fit assumes a regression coefficient, $R^2 = 0.973$ in the concentration range of 1 zM - 1 μM. The error values incorporated with the data points in linear fitting approximation are mean deviated values. As shown in Fig. 4(b), we plotted peak currents against target concentration, and fitted the response pattern with a four parameter logistic sigmoidal function as described earlier. Sensitivity of the biosensor towards atrazine detection in mineral water was found to be 6.33 (μA/μM)/cm^2 whereas the LOD was determined as 0.54 zM.

3.4.2. Detection of atrazine in ground water

To prepare the aliquots of atrazine, we followed a similar protocol as mentioned in the previous section. The electrochemical response of the bioelectrode to the addition of atrazine to bulk electrolyte was also recorded with DPV. As observed in the previous case of atrazine detection in mineral water, here also, upon increasing the concentration of atrazine, the overall peak current decreased significantly and the potential corresponding to peak current shifted to higher Values. Fig. 4(c) shows the resulting differential pulse voltagramm of the bioelectrode for different.

Target concentrations, along with a linear fitting approximation (inset). The linear curve fitting presented here assumes a regression coefficient $R^2 = 0.988$ in the target range 1 zM −1 μM. The error values associated with the data points in linear fitting approximation are mean deviated values. The dose-response behavior, along with a sigmoidal curve fitting approximation, for the detection of atrazine in ground water is presented in Fig. 4(d). As calculated, sensitivity and LOD of the sensor towards atrazine detection in ground water are 4.45 (μA/μM)/cm^2 and 0.84 zM respectively.

3.5. Stability, selectivity, interference test

Stability, selectivity and interference analysis are key to determine the efficiency of any sensor. Herein, in order to assess the stability of the proposed electrode after antibody immobilization, GCE/SnO_2/MPA/EDC-NHS/Antibody/BSA was stored for 4 weeks at 4 °C. The electrode's response was recorded periodically every 7 days and differential pulse voltammograms for the bioelectrode corresponding to different storage durations are presented in Fig. 5(a). DPV peak current was compared against the peak current recorded prior to so as to obtain the percentage change in signal strength. As shown in Fig. 5(b), there is 19% (n = 4, % RSD = 2.5) change in the peak current after 28 days of storage, indicating reasonable stability of the sensor. Selectivity of proposed sensor was investigated against Antibiotic (Amoxicillian), Urea, Glucose, BSA, HSA, Na^+ and Melamine, which were diluted in PBS (1 mM pH = 7.4) to prepare the target aliquots. Fig. 5(c) shows the electrochemical response of the bioelectrode against 1 μM aliquots of above mentioned compounds. We compared the recorded values to the sensor's response to 1 μM atrazine to evaluate the selectivity. The % change in peak current for ANTB (Antibiotic), Urea, Glucose, BSA, HSA, Na^+,

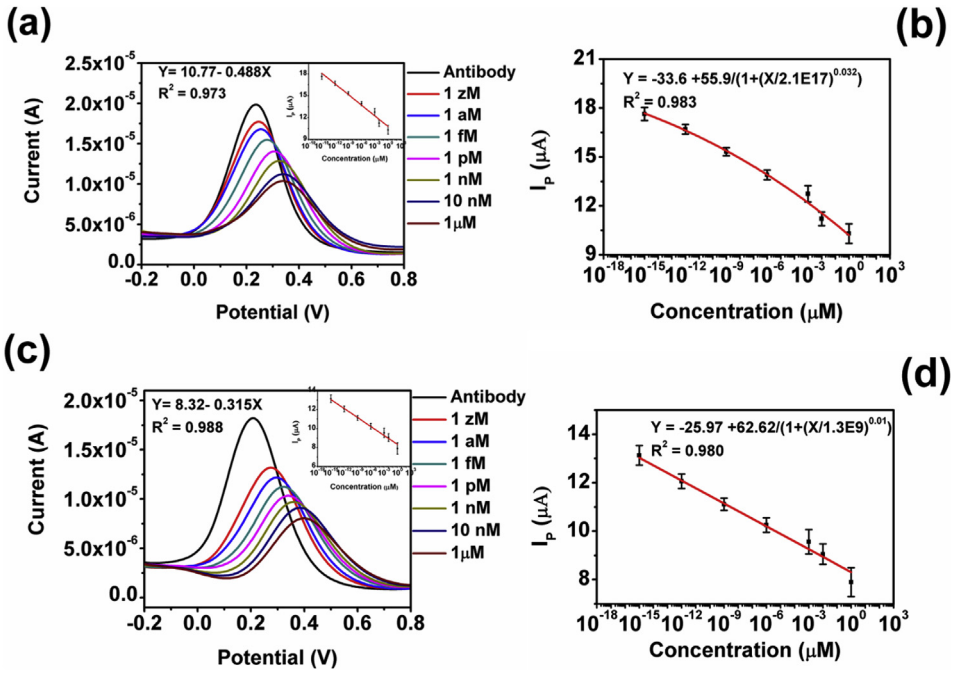

Fig. 4. (a) DPV of bioelectrode as function of atrazine diluted in **Mineral water** along with inset linear fitting of peak currents (b) Calibration curve of peak currents with logistic sigmoidal curve fitting (c) DPV of bioelectrode as function of atrazine diluted in **Ground water** along with inset linear fitting of peak currents (d) Calibration curve of peak currents with logistic sigmoidal curve fitting.

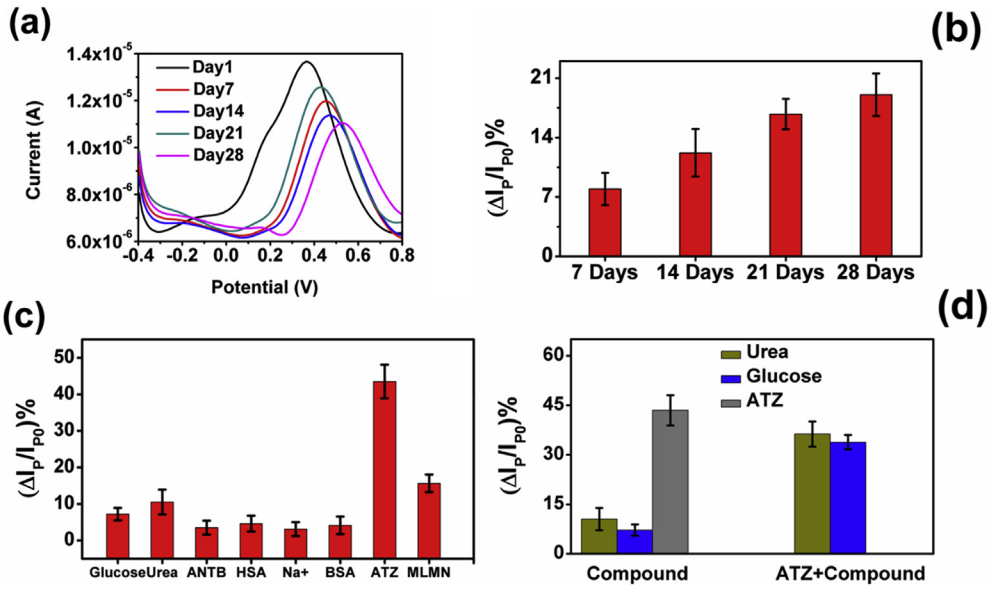

Fig. 5. (a) Variation of DPV peak currents with storage of antibody immobilized electrode for 4 weeks (b) Bar diagram representation of % change in peak currents for 4 weeks (n = 4) (c) Selectivity analysis - Bar diagram representation of % change in peak currents for different compounds (n = 4) (d) Interference analysis - Bar diagram representation of % change in peak currents for glucose, urea for addition of 1 μM pure compound, pure atrazine, (atrazine + compound) 1:1 ratio (n = 4).

Melamine and atrazine is 3.5 (n = 4, %RSD = 1.9), 10.5 (n = 4, %RSD = 3.4), 7.2 (n = 4, %RSD = 1.7), 4.1 (n = 4, %RSD = 2.4), 4.6 (n = 4, %RSD = 2.2), 3.1 (n = 4, %RSD = 1.9), 15.6 (n = 4, %RSD = 2.4) and 43.5 (n = 4, %RSD = 4.6) respectively. As can be inferred, even for a very high concentration of the non-specific targets, the sensor response is poor when compared to that with atrazine, indicating high degree of selectivity. We have performed interference studies for the bioelectrode in presence of two interfering compounds, namely urea and glucose. Towards this, we separately recorded the sensor's response to 1 μM of the interfering compound and 1 μM of atrazine. Then we exposed the biosensor to a 1:1 mixture of atrazine and the interfering compound, and recorded the response. Fig. 5(d) shows the percentage change in the anodic peak currents of DPV responses of the bioelectrode, for different target conditions. As can be seen, for an identical target concentration, the percentage change in peak currents for urea is 10.5% (n = 4, %RSD = 3.4) as opposed to 43.5% (n = 4, %RSD = 4.6) for atrazine. In presence of a 1:1 mixture of atrazine and urea, the bioelectrodes response accounts for a 36.3% (n = 4, %RSD = 3.8) change in peak current. A similar trend can be seen in presence of glucose also, wherein the sensor's response to a 1:1 mixture of atrazine and urea matches closely to the response recorded against atrazine.

4. Conclusions

In this work, we have demonstrated facile synthesis of electrospun tin oxide nanofibers which were later used for developing an ultrasensitive electrochemical platform for the detection of atrazine in water. Properties of the synthesized nanomaterial were studied using high-end characterization techniques such as FESEM, XPS, XRD, UV-Vis-NIR Spectroscopy and FTIR spectroscopy. The electrochemical biosensor developed in this study results in sensitivity of 4.11 (μA/μM)/cm^2 and LOD of 0.9 zM in the detection range of 1 zM −1 μM. The sensor accounts for reasonable stability and excellent selectivity. Additionally, in presence of interfering compounds such as urea and glucose, the sensor's ability to detect atrazine remains nearly unaffected. In view of practical applications, we have subjected the proposed platform to atrazine detection in spiked ground and mineral water, which resulted in LOD of 0.84 zM and 0.54 zM respectively. This is a clear indication that the proposed sensor can be implemented for atrazine detection in real-time water samples.

The future work of the proposed research is directed towards miniaturization of the propose platform, so as to develop a handheld portable device which can be deployed at remote locations for atrazine detection. Furthermore, the device can be linked with IoT infrastructures such that continuous monitoring of atrazine level in water can be performed along with data-sharing via wireless sensor networks.

Declarations of interest

The authors declare that there is no declaration of interest in relation to this work, and the publication.

CRediT authorship contribution statement

Patta Supraja: Conceptualization, Data curation, Formal analysis, Investigation, Validation, Writing - original draft. **Suryasnata Tripathy:** Validation, Methodology, Writing - original draft. **Siva Rama Krishna Vanjari:** Resources, Writing - review & editing. **Vikrant Singh:** Methodology, Validation. **Shiv Govind Singh:** Supervision, Resources, Funding acquisition, Writing - review & editing.

Acknowledgements

The authors acknowledge Department of Science and Technology (Fund for Improvement of S&T infrastructure), Government of India for funding research. Parts of the reported work (Nanomaterial characterization) were carried out at the Indian Institute of Technology, Bombay under the Indian Nano electronics Users Program, which is sponsored by Department of Electronics and Information Technology (DEITY), Ministry of Communications and Information Technology, the Government of India.

Appendix A. Supplementary data

Supplementary data to this article can be found online at https://doi.org/10.1016/j.bios.2019.111441.

References

Agrawal, H., Shrivastav, A.M., Gupta, B.D., 2016. Sensor. Actuator. B Chem. 227, 204–211.
Aktar, M.W., Sengupta, D., Chowdhury, A., 2009. Interdiscip. Toxicol. 2, 1–12.
Amiri, S., Navaee, A., Salimi, A., Ahmadi, R., 2017. Electrochem. Commun. 78, 21–25.
Brince Paul, K., Kumar, S., Tripathy, S., Vanjari, S.R.K., Singh, V., Singh, S.G., 2016. Biosens. Bioelectron. 80, 39–46.
Cheng, L., Ma, S.Y., Wang, T.T., Li, X.B., Luo, J., Li, W.Q., Mao, Y.Z., GZ, D.J., 2014. Mater. Lett. 131, 23–26.

Dharmaraj, N., Kim, C.H., Kim, K.W., Kim, H.Y., Suh, E.K., 2006. Spectrochim. Acta Part A Mol. Biomol. Spectrosc. 64, 136–140.
Dou, X., Mathews, N., Wang, Q., Pramana, S.S., Lam, Y.M., Mhaisalkar, S., 2011. Nanoscale 3, 4640–4646.
Farré, M., Martínez, E., Ramón, J., Navarro, A., Radjenovic, J., Mauriz, E., Lechuga, L., Marco, M.P., Barceló, D., 2007. Anal. Bioanal. Chem. 388, 207–214.
Fu, B., Van Dyck, C., Zaleski, S., Van Duyne, R.P., Ratner, M.A., 2016. J. Phys. Chem. C 120, 27241–27249.
Grennan, K., Strachan, G., Porter, A.J., Killard, A.J., Smyth, M.R., 2003. Anal. Chim. Acta 500, 287–298.
Hartley, D., Kidd, H., 1987. The Agrochemicals Handbook, second ed. Royal Society of Chemistry Cambridge.
Helali, S., Martelet, C., Abdelghani, A., Maaref, M.A., Jaffrezic-Renault, N., 2006. Electrochim. Acta 51, 5182–5186.
Ionescu, R.E., Gondran, C., Bouffier, L., Jaffrezic-Renault, N., Martelet, C., Cosnier, S., 2010. Electrochim. Acta 55, 6228–6232.
Javaroni, R. de C.A., Landgraf, M.D., Rezende, M.O.O., 1999. QuÃ\-mica Nov 22, 58–64.
Jia, K., Adam, P.-M., Ionescu, R.E., 2013. Sensors Actuators B Chem 188, 400–404.
Keay, R.W., McNeil, C.J., 1998. Biosens. Bioelectron. 13, 963–970.
Kolpin, D.W., Barbash, J.E., Gilliom, R.J., 2000. Pesticides in ground water of the United States, 1992–1996. Groundwater 38, 858–863.
Maleki, N., Absalan, G., Safavi, A., Farjami, E., 2007. Anal. Chim. Acta 581, 37–41.
Mazzei, F., Botre, F., 2007. Int. J. Environ. Heal. 1, 185–198.
Nehru, L.C., Sanjeeviraja, C., 2014. J. Adv. Ceram. 3, 171–176.
Neumann, G., Teras, R., Monson, L., Kivisaar, M., Schauer, F., Heipieper, H.J., 2004. Appl. Environ. Microbiol. 70, 1907–1912.
Panuwet, P., Nguyen, J.V., Kuklenyik, P., Udunka, S.O., Needham, L.L., Barr, D.B., 2008. Anal. Bioanal. Chem. 391, 1931.
Penmetsa, K.V., Leidy, R.B., Shea, D., 1996. J. Chromatogr. A 745, 201–208.
Rahi, A., Sattarahmady, N., Heli, H., 2015. Sci. Rep. 5, 18060.
Ramón-Azcón, J., Valera, E., Rodríguez, Á., Barranco, A., Alfaro, B., Sanchez-Baeza, F., Marco, M.-P., 2008. Biosens. Bioelectron. 23, 1367–1373.
Reardon, K.F., 2012. Anal. Lett. 45, 251–261.
Saylan, Y., Akgönüllü, S., Çimen, D., Derazshamshir, A., Bereli, N., Yılmaz, F., Denizli, A., 2017. Sensors Actuators B Chem 241, 446–454.
Shiu, W.Y., Ma, K.C., Mackay, D., Seiber, J.N., Wauchope, R.D., 1990. Springer New York, New York, NY, pp. 15–187.
Smith, A.M., Lee, A.A., Perkin, S., 2016. J. Phys. Chem. Lett. 7, 2157–2163.
Stern, E., Wagner, R., Sigworth, F.J., Breaker, R., Fahmy, T.M., Reed, M.A., 2007. Nano Lett 7, 3405–3409.
Supraja, P., Tripathy, S., Krishna Vanjari, S.R., Singh, V., Singh, S.G., 2019. Sensors Actuators B Chem 285, 317–325.
Tang, W., Jiang, G., Cai, Z., 2005. Int. J. Environ. Anal. Chem. 85, 1117–1125.
Trachta, G., Schwarze, B., Sägmüller, B., Brehm, G., Schneider, S., 2004. J. Mol. Struct. 693, 175–185.
Tripathy, S., Krishna Vanjari, S.R., Singh, V., Swaminathan, S., Singh, S.G., 2017. Biosens. Bioelectron. 90, 378–387.
Vogel, A., Jocque, H., Sirot, L.K., Fiumera, A.C., 2015. J. Insect Physiol. 72, 14–21.
Williams, D.B.G., George, M.J., Marjanovic, L., 2014. J. Agric. Food Chem. 62, 7676–7681.
Yokley, R.A., Cheung, M.W., 2000. J. Agric. Food Chem. 48, 4500–4507.